Chemical Reaction Engineering

Heterogeneous reactions

Jayant M. Modak
Department of Chemical Engineering
Indian Institute of Science, Bangalore

Topic 6: Heterogeneous reactions

- Gas-solid catalytic reactions
- Gas-solid noncatalytic reactions
- Gas-liquid reactions

Heterogeneous catalysis

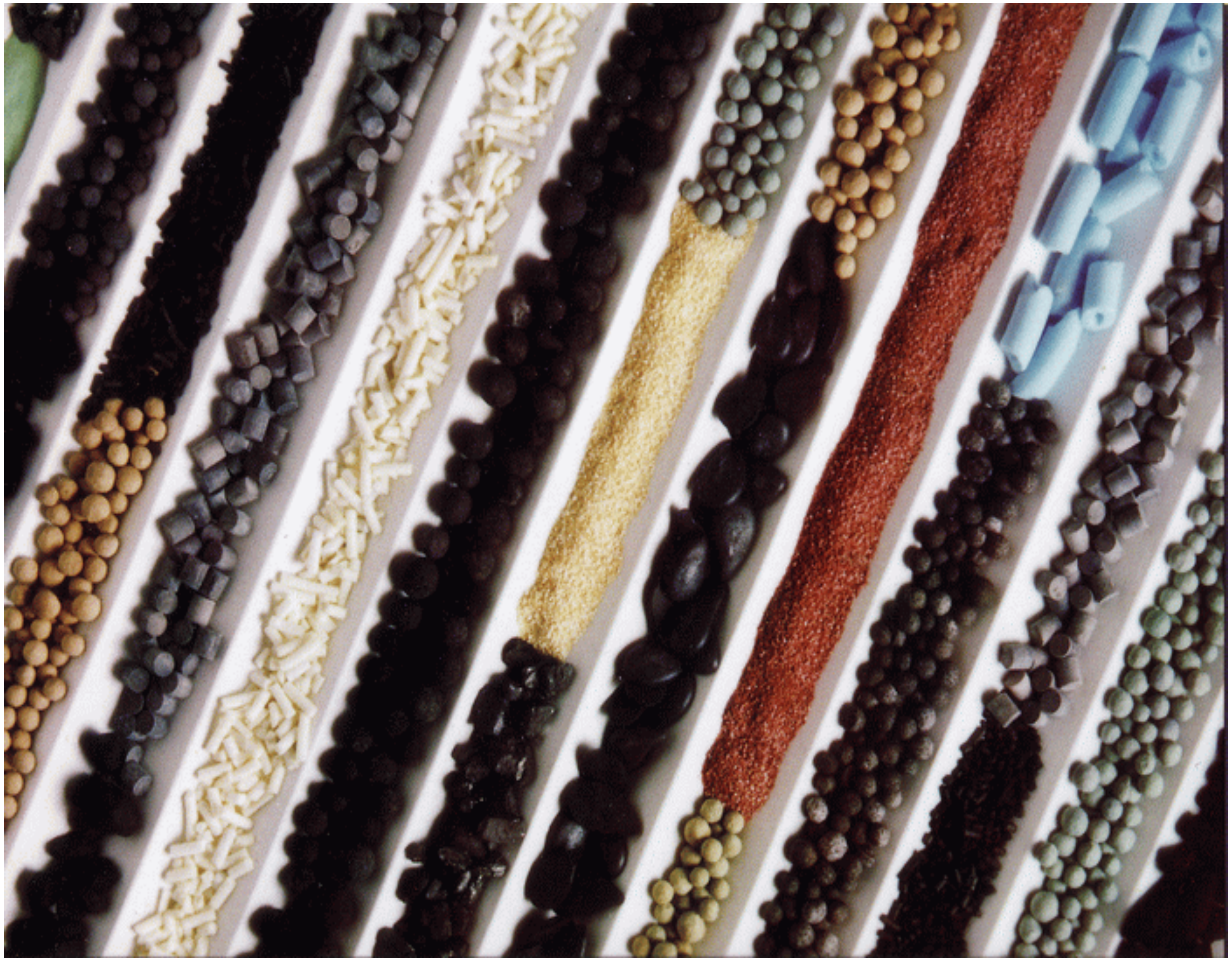

Heterogeneous catalysis

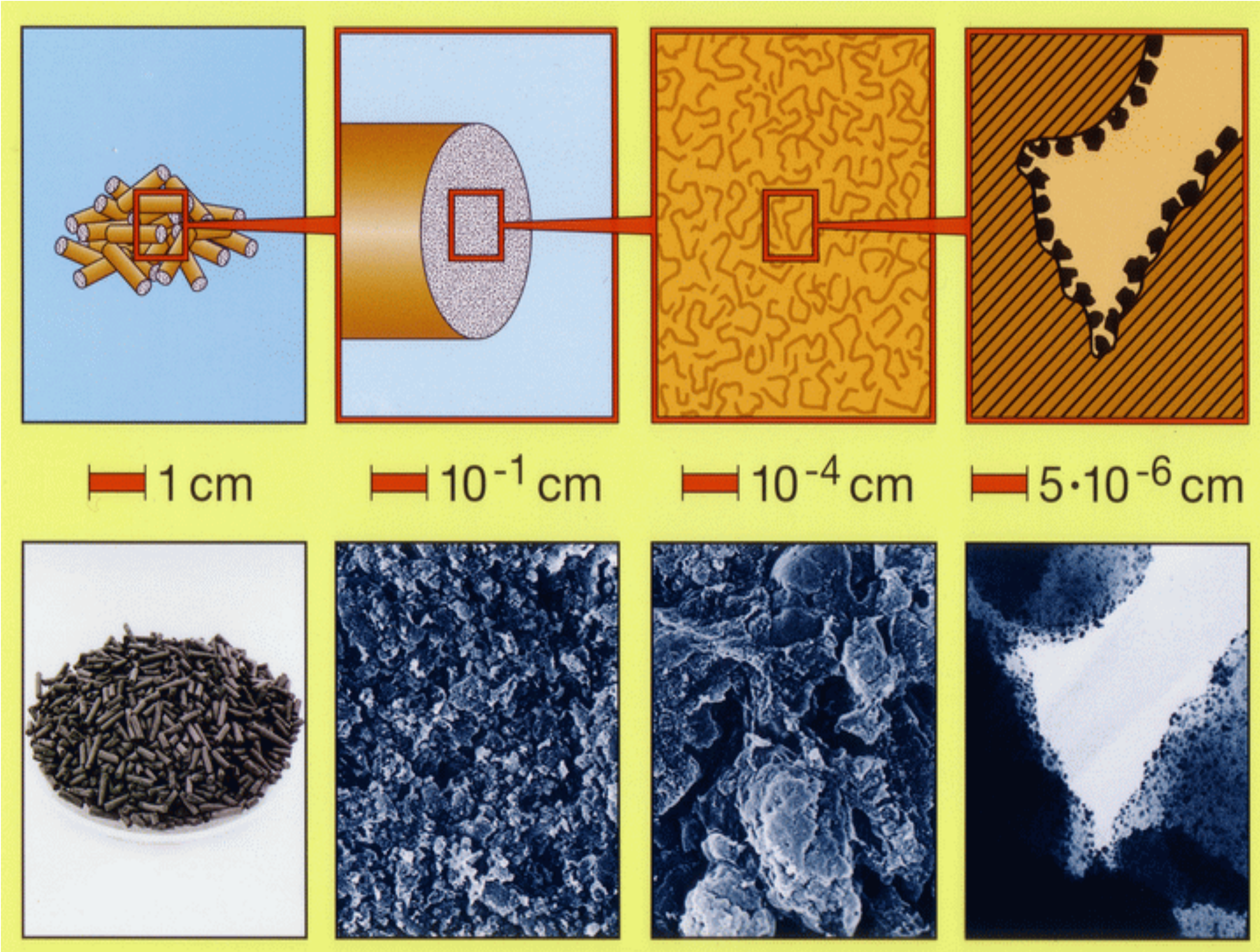

Concentration and temperature profiles

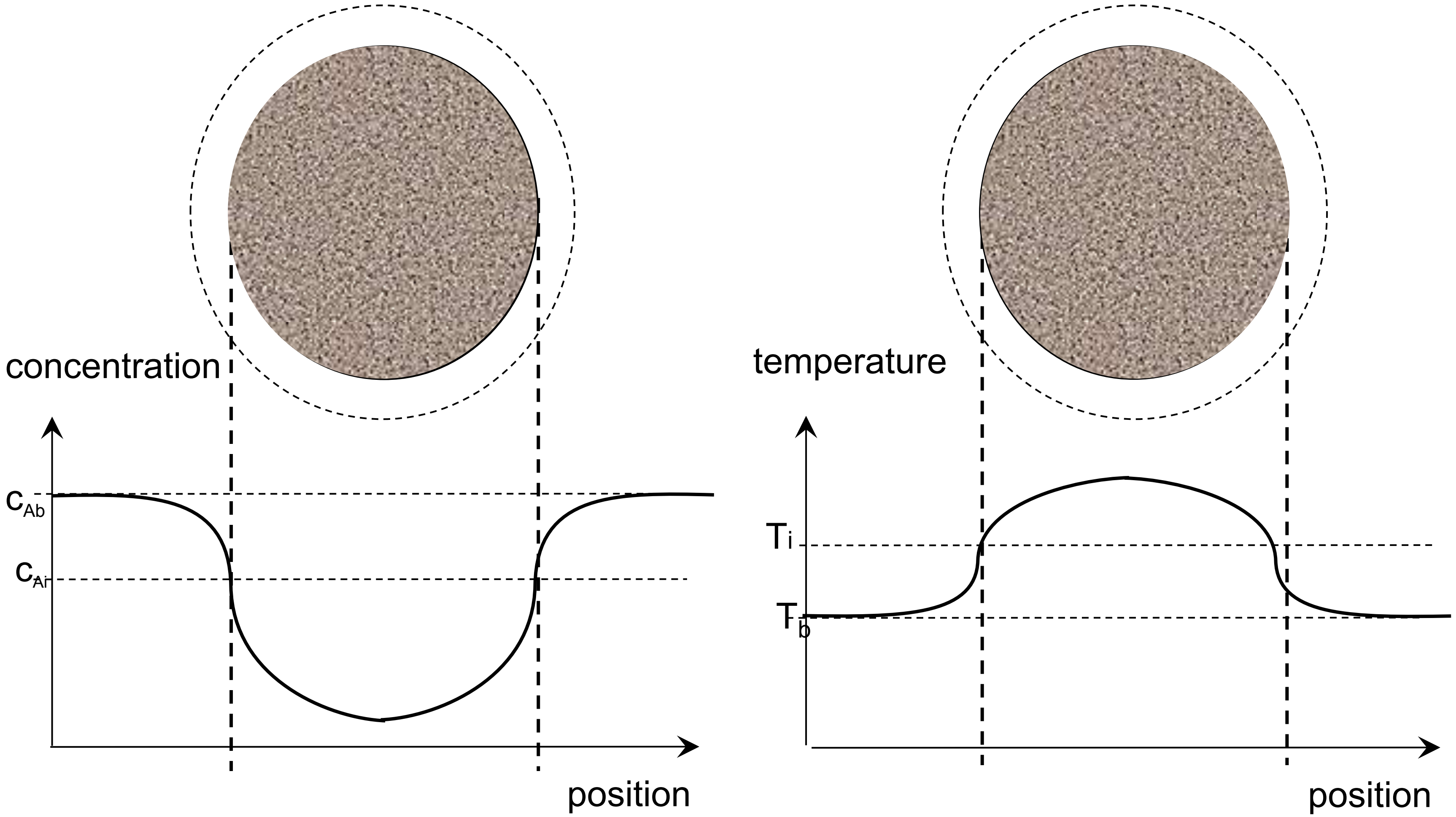

External transport

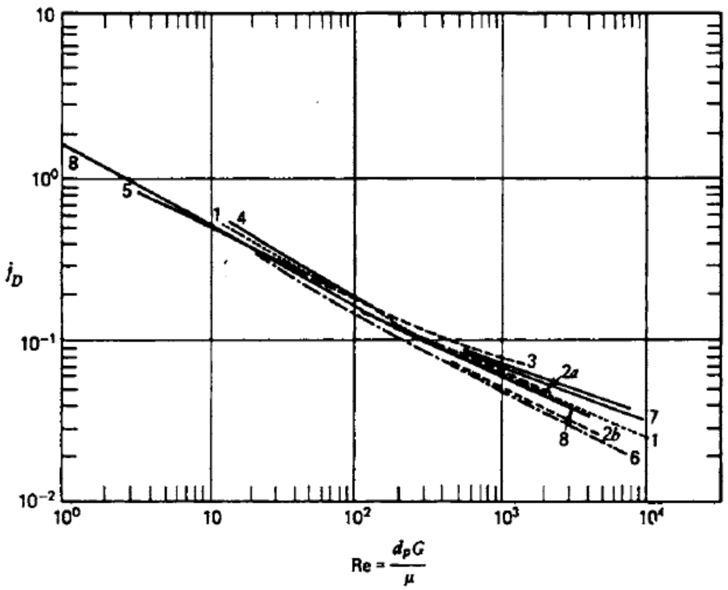

Figure 3.2.a-1 Mass transfer between a fluid and a bed of particles. Curve 1: Gamson et al. [3], *Wilke and Hougen* [4]. *Curve 2: Taecker and Hougen* [5]. *Curve 3: McCune and Wilhelm* [6]. *Curve 4: Ishino and Otake* [7]. *Curve 5: Bar Ilan and Resnick* [8]. *Curve 6: De Acetis and Thodos* [9]. *Curve 7: Bradshaw and Bennett* [10]. *Curve 8: Hougen* [11]; *Yoshida, Ramaswami, and Hougen* [12] *(spheres; $\varepsilon = 0.37$).*

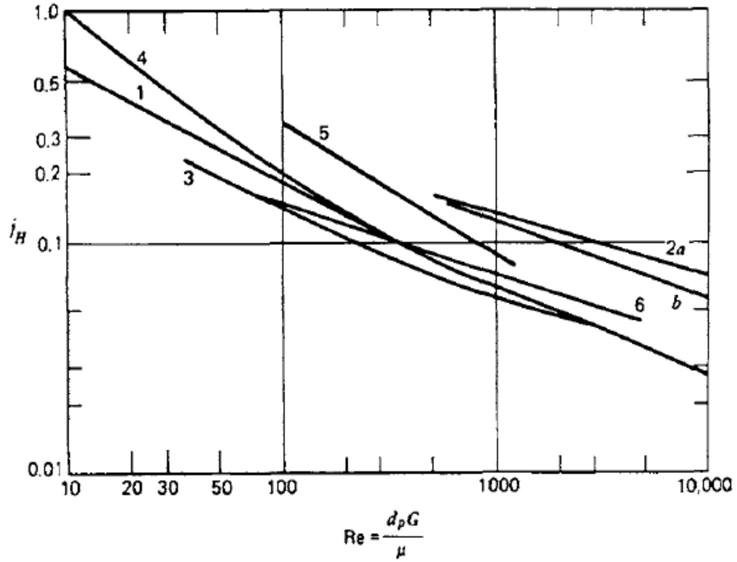

Figure 3.2.b-1 Heat transfer between a fluid and a bed of particles. Curve 1: Gamson et al., Wilke and Hougen [3, 4]. *Curve 2: Baumeister and Bennett (a) for $d_t/d_p > 20$, (b) mean correlation* [13]. *Curve 3: Glaser and Thodos* [14]. *Curve 4: de Acetis and Thodos* [9]. *Curve 5: Sen Gupta and Thodos* [15]. *Curve 6: Handley and Heggs* [16] *($\varepsilon = 0.37$).*

Bulk/Molecular diffusion

Binary

$$D_{12} = \frac{1.86\times10^{-3} T^{3/2}\left(\frac{1}{M_1} + \frac{1}{M_2} \right)^{1/2}}{P\sigma_{12}^2 \Omega} \quad \left[gases: 10^{-1}\ ; liquids: 10^{-5}\ cm^2/s \right]$$

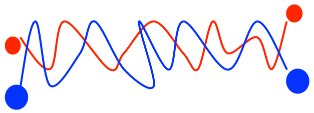

$$N_1 = -D_{12} C_T \nabla y_1 + y_1 \left(N_1 + N_2 \right)$$

Multi-component

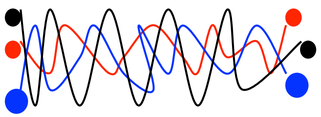

$$N_j = -D_{jm} C_T \nabla y_j + y_j \sum_{k=1}^{N} N_k \qquad D_{jm} = \frac{\sum_{k\neq j}^{N} \frac{1}{D_{jk}} \left(y_k - y_j \frac{N_k}{N_j} \right)}{1 - y_j \sum_{k=1}^{N} N_k / N_j}$$

Characterization of catalyst pellet

S_g *surface area / gm catalyst*

V_g *void volume / gm catalyst*

ρ_p *gm catalyst / pellet volume*

ε_p *void fraction*

$f(r)dr$ *void volume distribution*

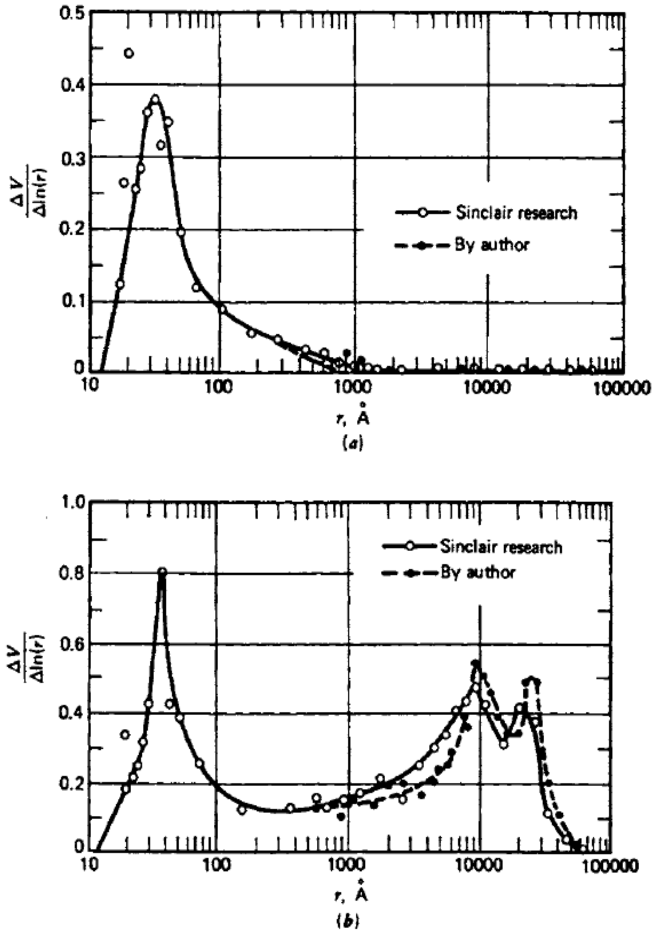

Figure 3.4-1 Pore-size distribution in catalyst pellets. (*a*) *Pellet 2.* (*b*) *Pellet 1.* (*From Cunningham and Geankoplis* [28].)

Transport in pore

Bulk 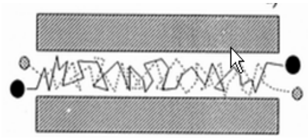 Knudson 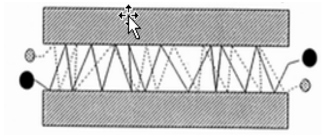 Viscous 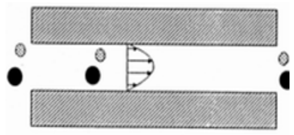

$$-\frac{1}{RT}\nabla p_j = \sum_{k\neq j}^{N}\frac{1}{D_{jk}}\left(y_k N_j - y_j N_k\right) + \frac{N_j}{D_{Kj}} + \frac{y_j}{D_{Kj}}\left(\frac{PB_0}{RT\mu}\right)\nabla P$$

$$D_{Kj} = \frac{2}{3}\bar{r}\left(\frac{8RT}{\pi M_j}\right)^{1/2}$$

Transport in pellet

$$N_j = -D_{jm}\frac{dC_j}{dz}$$

$$N_j = -D_{ej}\frac{dC_j}{dz}$$

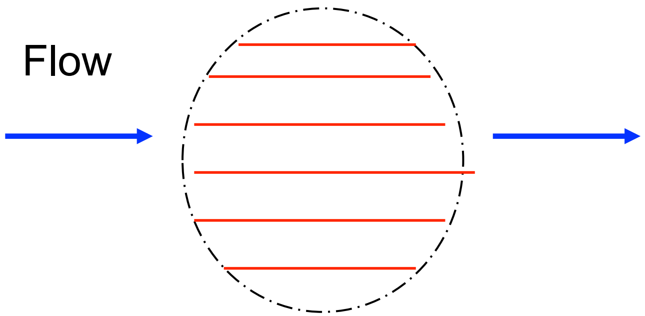

$$D_{ej} = \frac{\varepsilon}{\tau} D_{jm}$$

Reaction and diffusion A→B

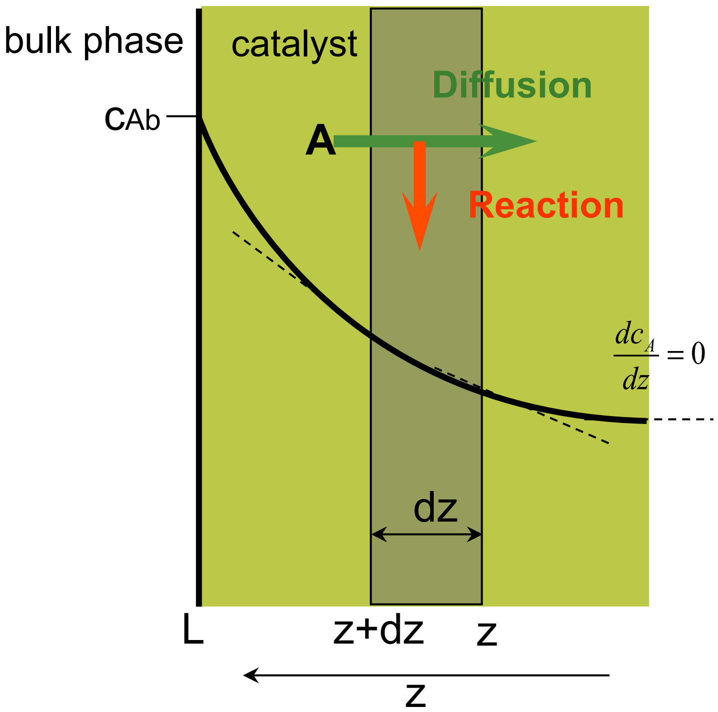

Accumulation	$C_A A_g dz\big\vert_{t+dt} - C_A A_g dz\big\vert_t$
In	$D_{eA} \frac{dC_A}{dz} A\Big\vert_{z+dz} dt$
Out	$D_{eA} \frac{dC_A}{dz} A\Big\vert_{z} dt$
Generated	$-r\, A dz\, dt$

$$\frac{\partial}{\partial t}\left(\varepsilon_p C_A\right) = \frac{\partial}{\partial z}\left(D_{eA} \frac{\partial C_A}{\partial z}\right) - r$$

Concentration profiles

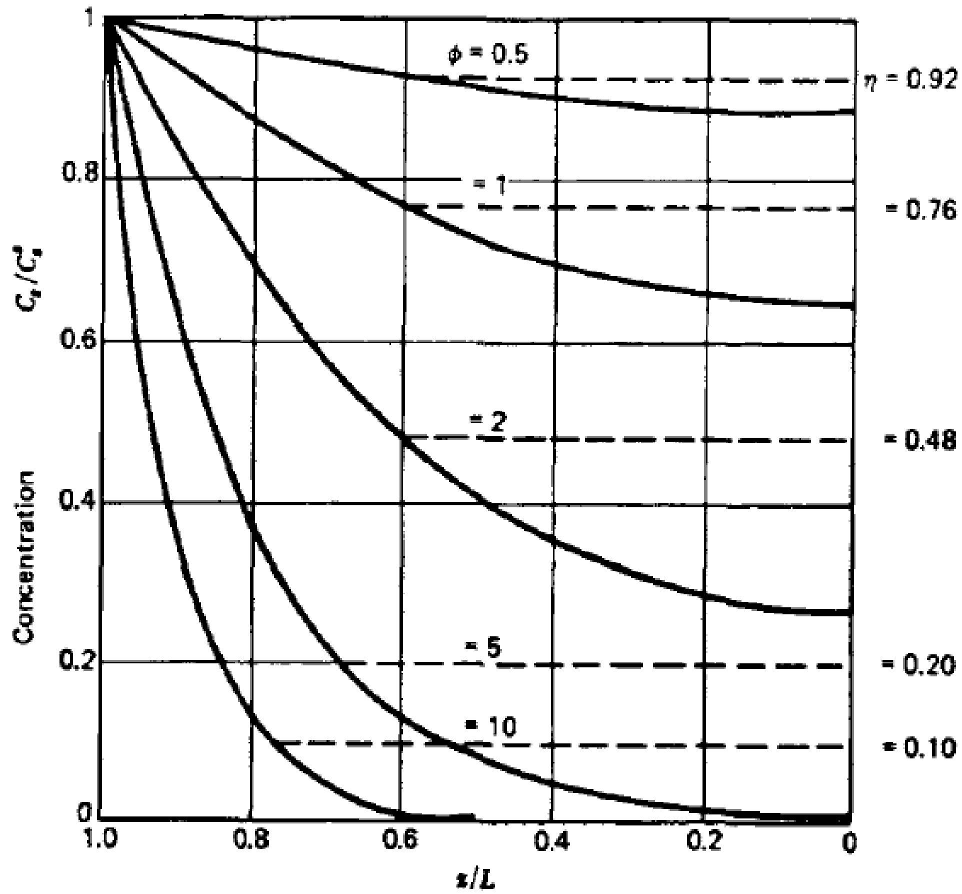

Figure 3.6.a-1 Distribution and average value of reactant concentration within a catalyst pore as a function of the parameter ϕ. (*Adapted from Levenspiel* [75].)

Effectiveness factor

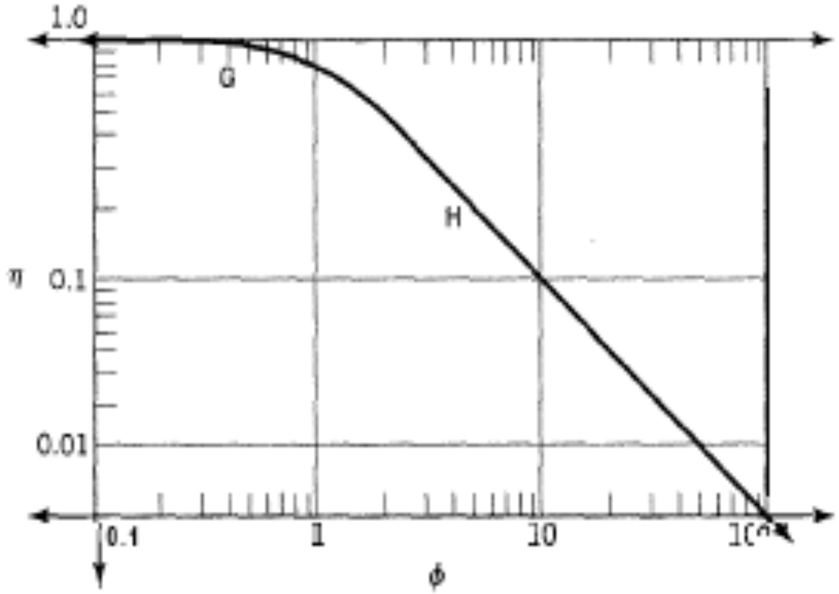

Figure 8.11 Effectiveness factor (η) as a function of Thiele modulus (ϕ) for an isothermal particle; three regions indicated:

Effect of geometry

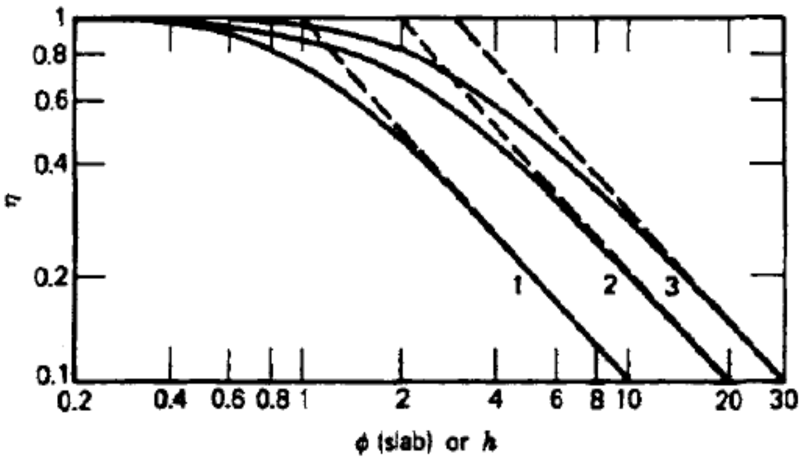

Figure 3.6.a-2 Effectiveness factors for (1) slab, (2) cylinder, and (3) sphere(from Aris [78].)

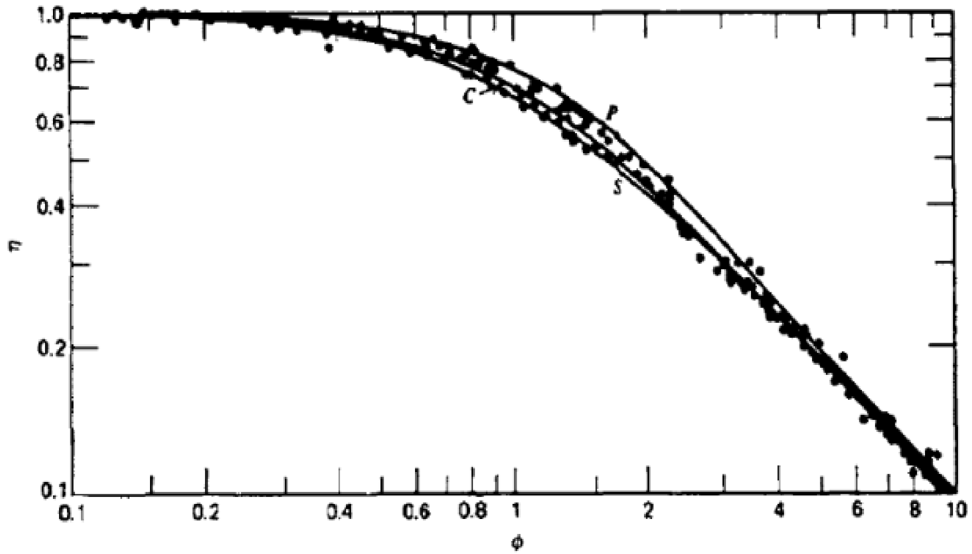

Figure 3.6.a-3 Effectiveness factors for slab, cylinder and sphere as functions of the Thiele modulus ϕ. The dots represent calculations by Amundson and Luss (1967) and Gunn (1967). (From Aris [74].)

Nonlinear kinetics

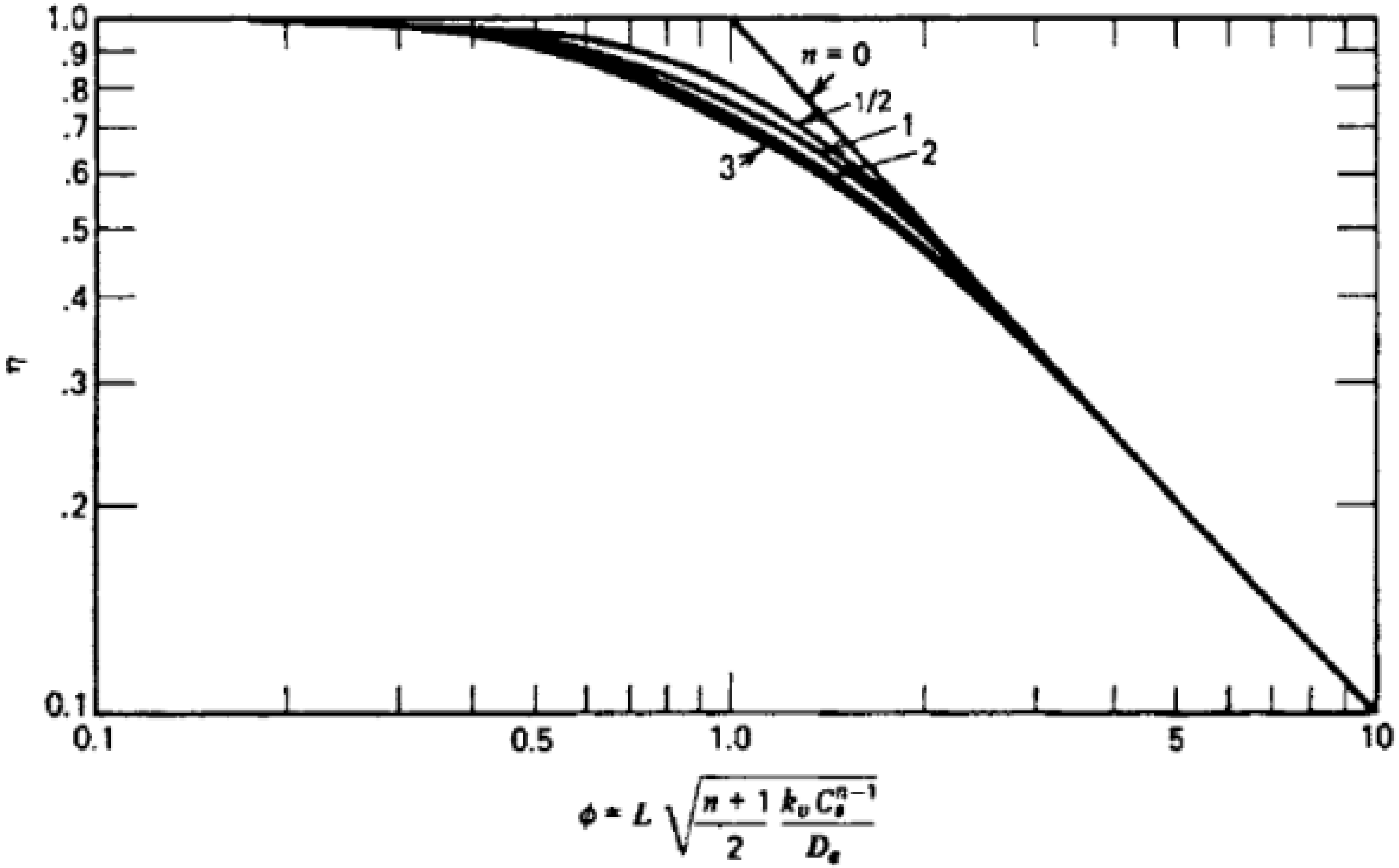

Figure 3.6.b-1 Generalized plot of effectiveness factor for simple order reactions.

Falsification of the kinetics

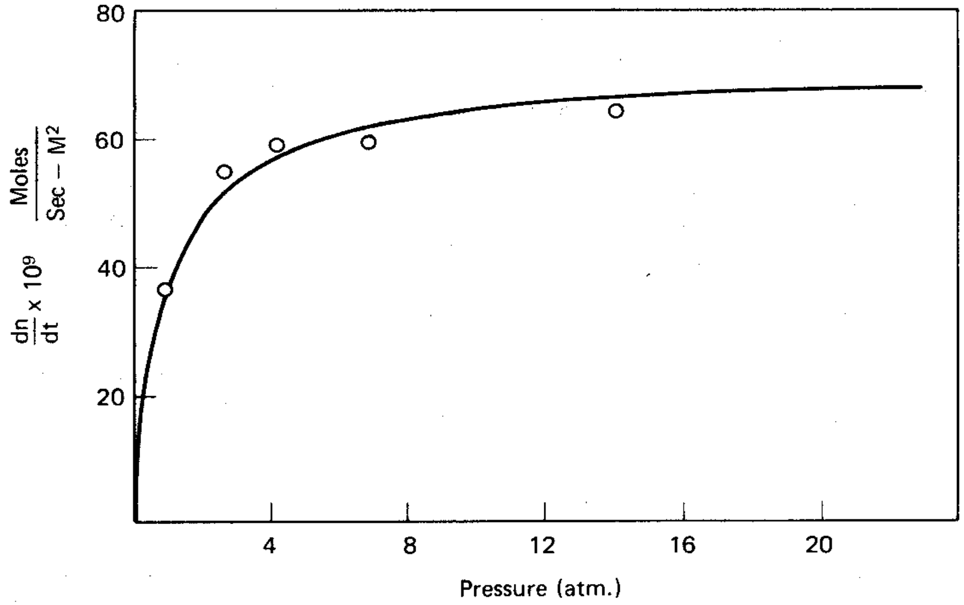

Figure 4.7. The Effect of Diffusion Transport on a Zeroth-Order Reaction. Pressure Dependence in the Cracking of Cumene on Silica Alumina. [After Weisz and Prater (1954)].

Falsification of the kinetics

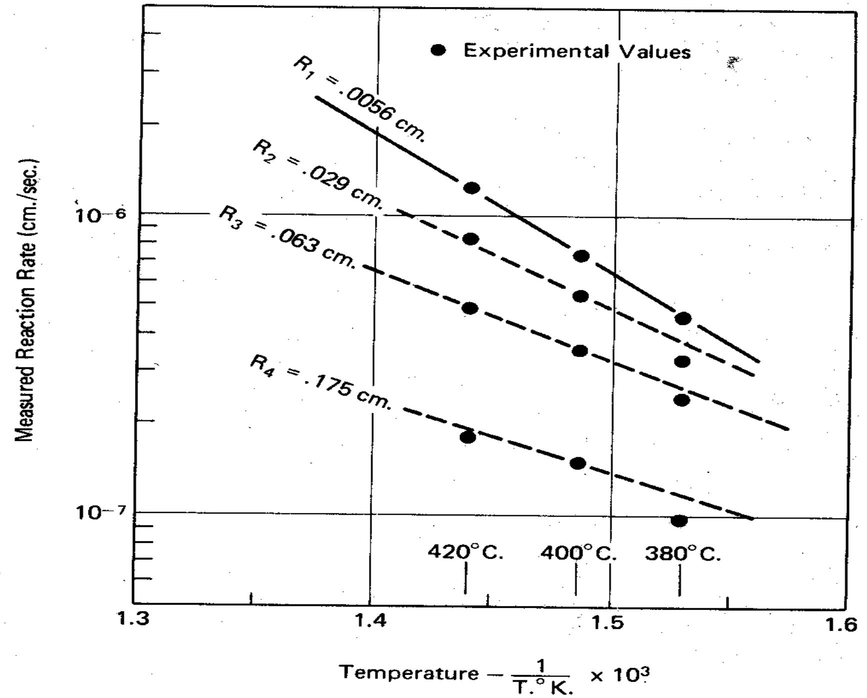

Figure 4.8. Experimental Demonstration of the Effect of Diffusion on the Measured Activation Energy of the Cracking of Cumene on SiO_2-Al_2O_3 Catalyst. [After Weisz and Prater (1954)].

Multiple reactions

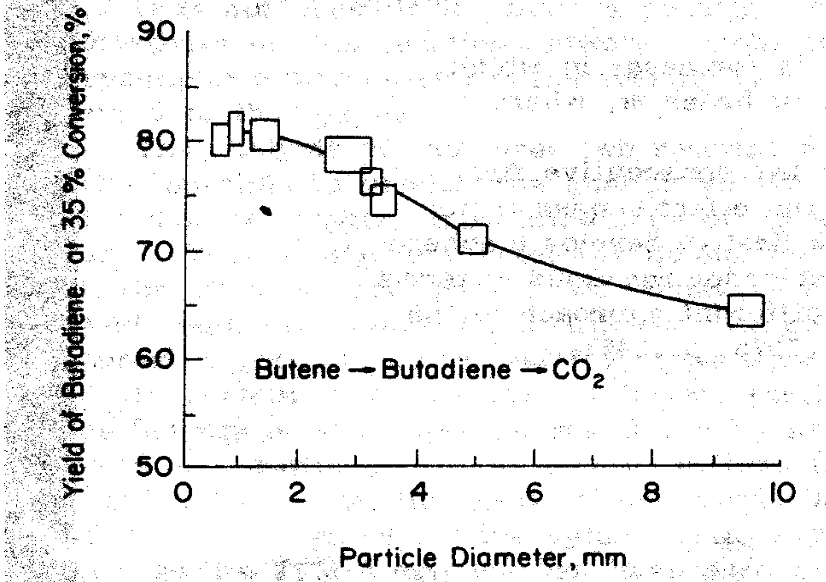

FIGURE 11 Dependence of the yield of butadiene on iron oxide catalyst particle size at 620°C. (From Voge and Morgan, 1972.)

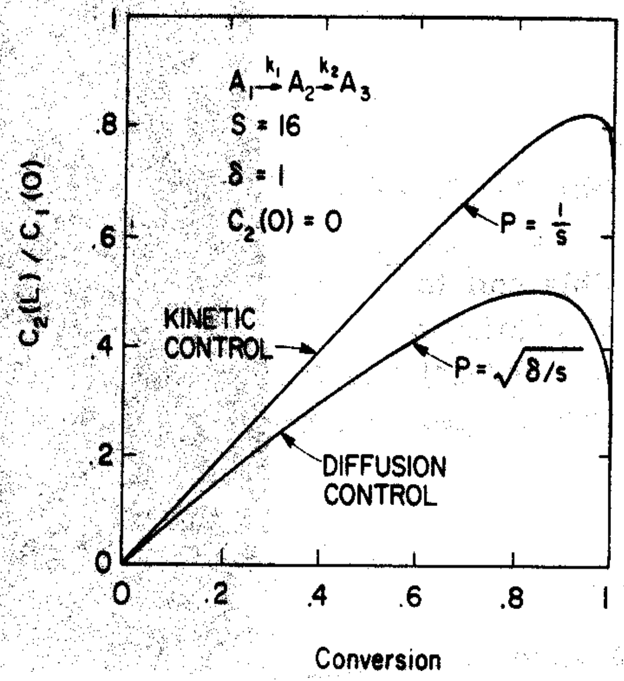

Nonisothermal pellet

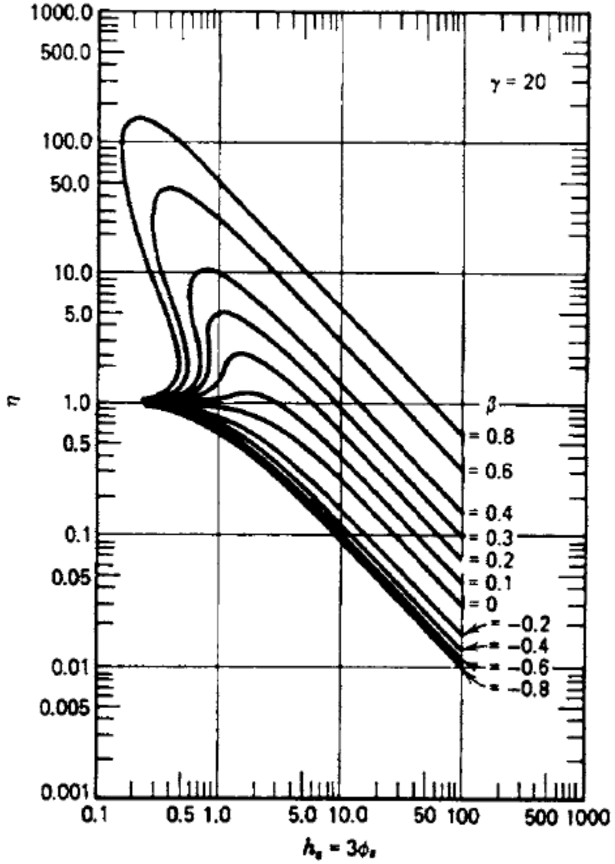

Figure 3.7.a-1 Effectiveness factor with first-order reaction in a spherical nonisothermal catalyst pellet (from Weisz and Hicks [112]).

Nonisothermal pellet

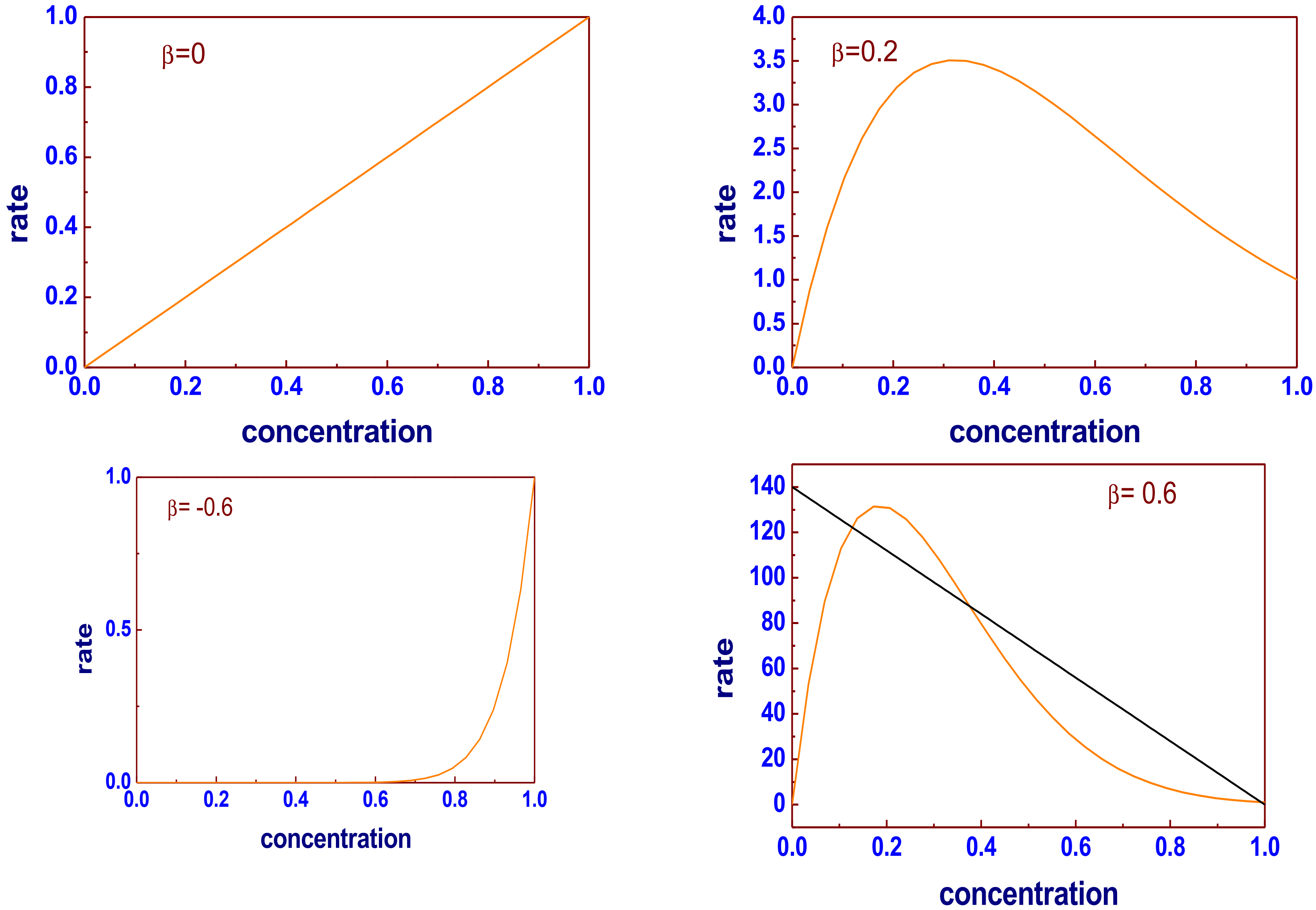

External and internal energy transfer limitations

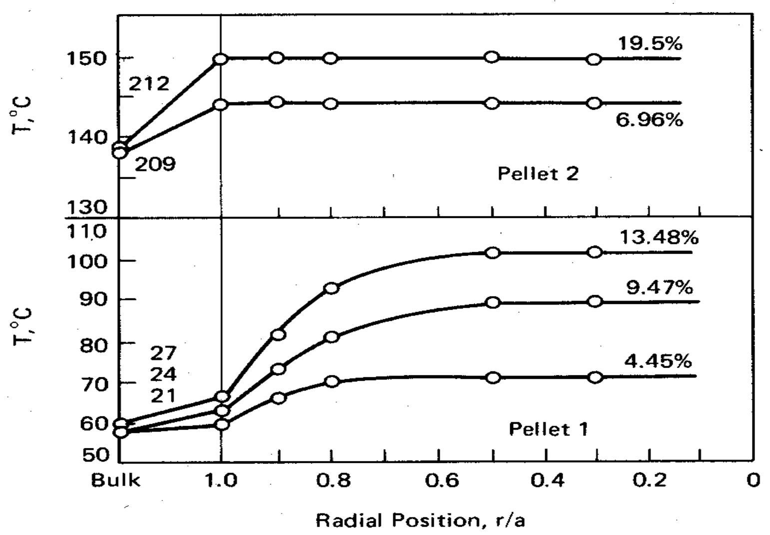

Figure 4.12, Measured Internal and External Temperature Profiles During the Hydrogenation of Benzene on Ni as a Function of Feed Composition for Two Pellets of Different Conductivities. [After Kehoe and Butt (1972)].

Multiple steady states and hysteresis

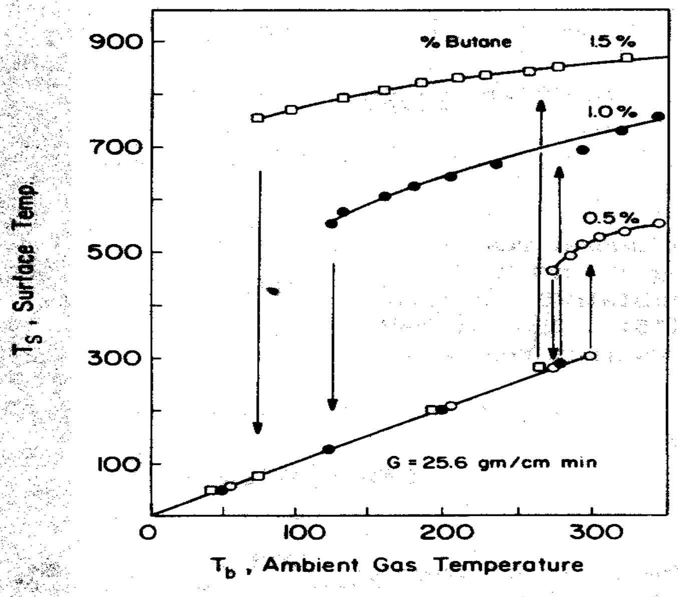

FIGURE 14 Dependence of catalyst wire surface temperatures on gas temperatures and butane concentrations. (From Cardoso and Luss, 1969.)

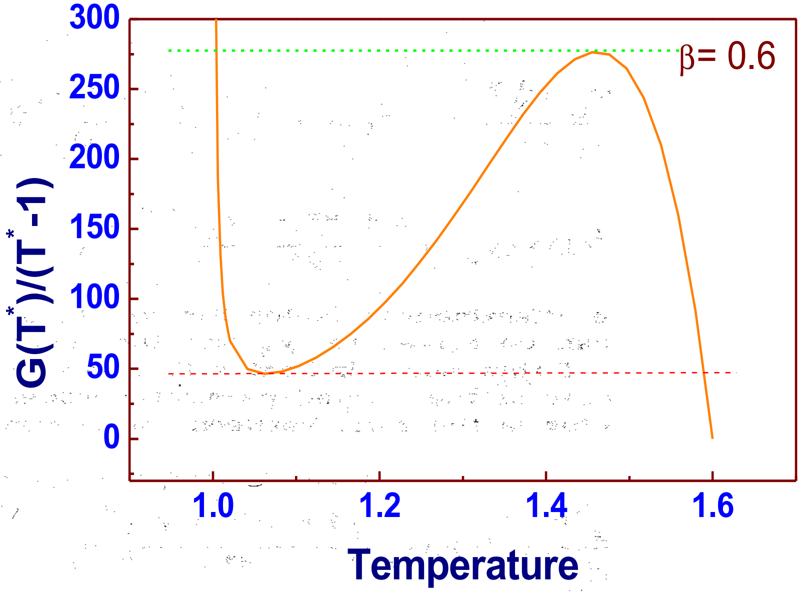

Gas-solid noncatalytic reactions

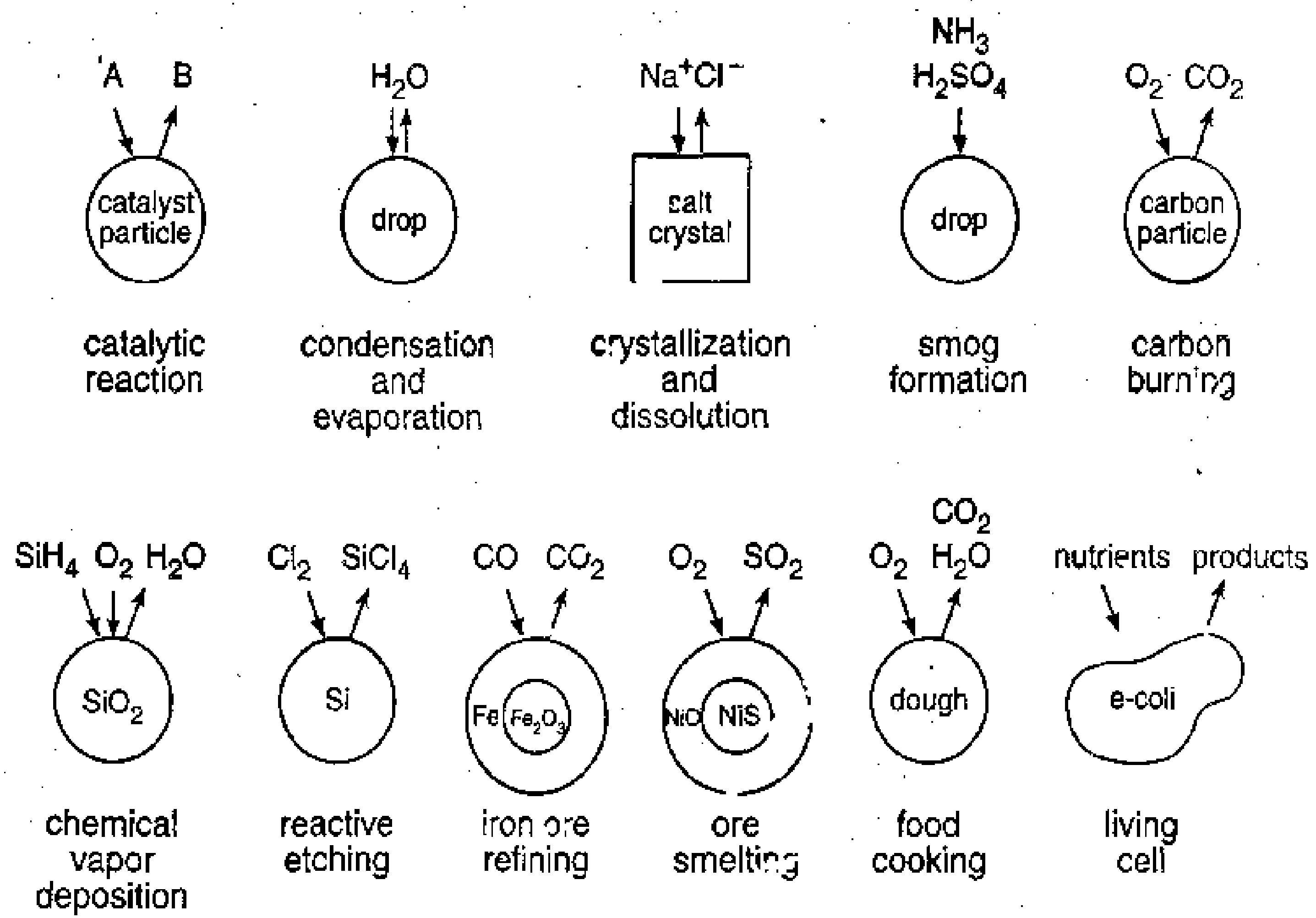

Figure 9–1 Examples of fluid–solid and fluid–liquid reactions of approximately spherical solid or liquid particles.

Gas-solid noncatalytic reactions

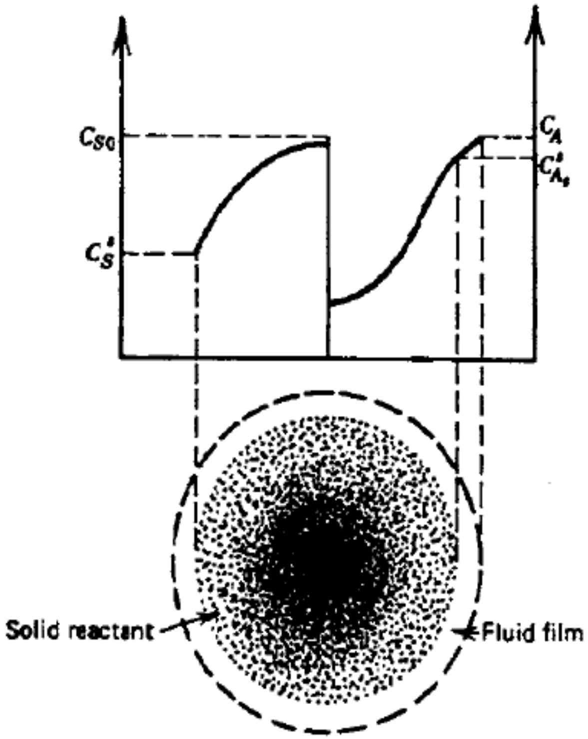

Figure 4.1-2 General model (from Wen [2]).

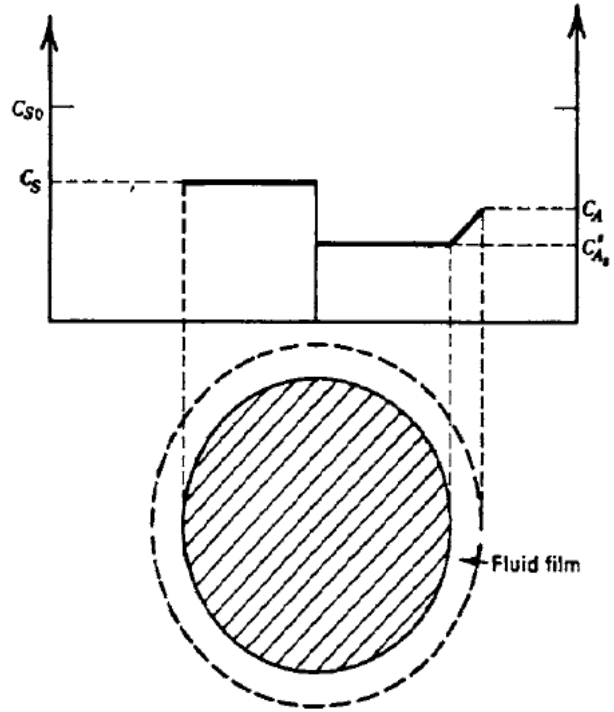

Figure 4.1-3 Truly homogeneous model. Concentration profiles (from Wen [2]).

Gas-solid noncatalytic reactions

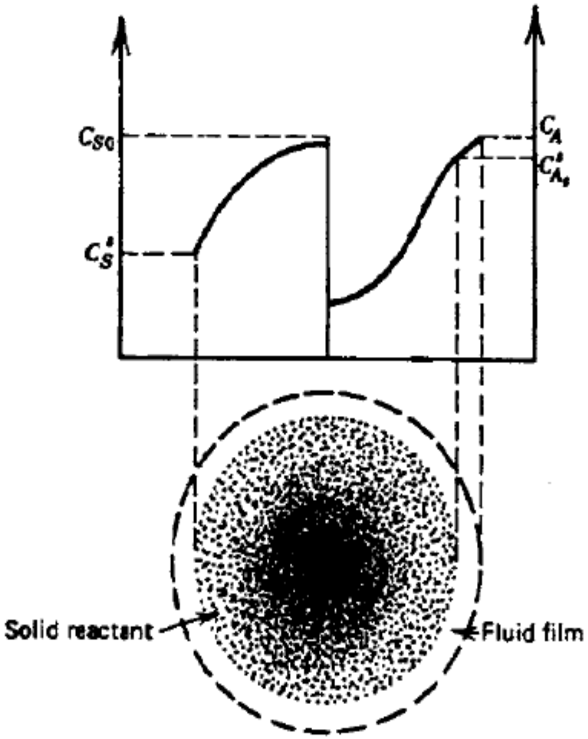

Figure 4.1-2 General model (from Wen [2]).

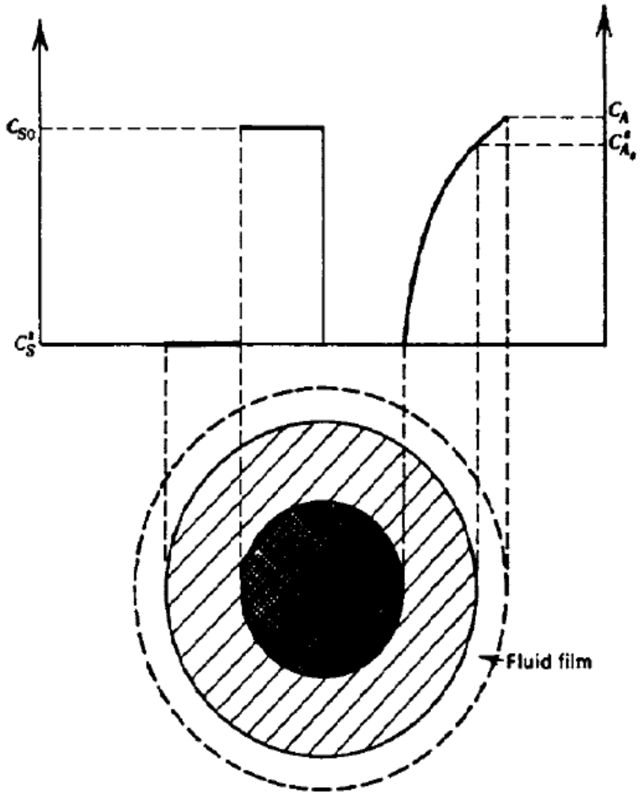

Figure 4.1-1 Heterogeneous shrinking core model with sharp interface. Concentration profiles of gas and solid reactants (from Wen [2]).

Shrinking particle model

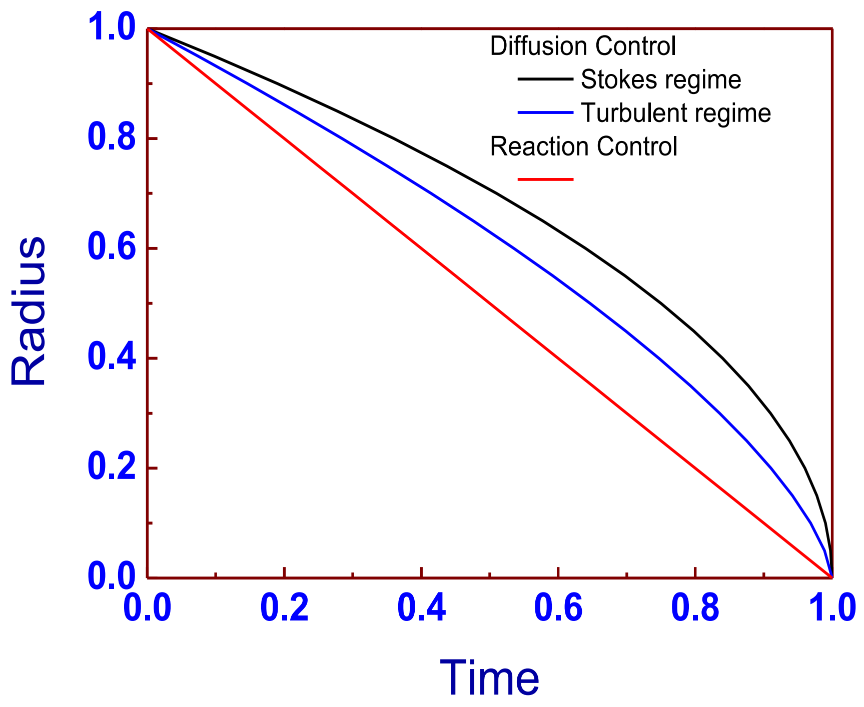

Shrinking unreacted core model

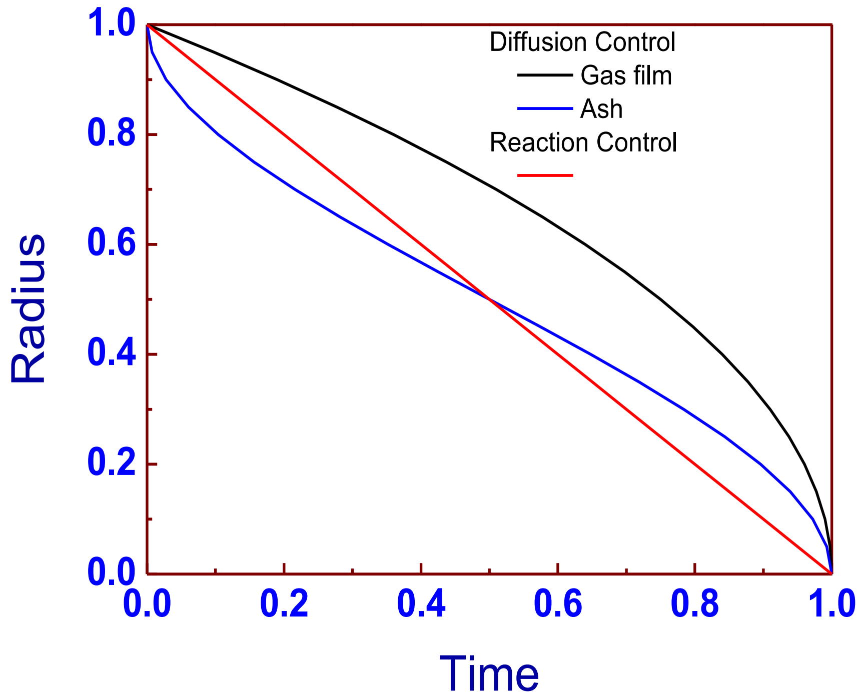

Burning of coke from alumina-silica catalyst

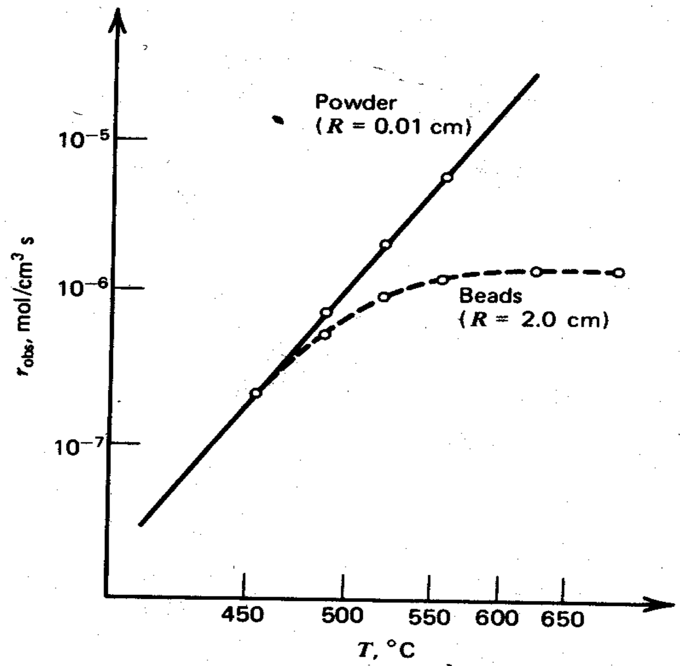

Figure 1
Average observed burning rates of conventional silica alumina cracking catalyst. Initial carbon content 3.4 wt-%. Beads (dashed line), and ground-up catalyst (full curve). From Weisz and Goodwin (1963).

Burning of coke from alumina-silica catalyst

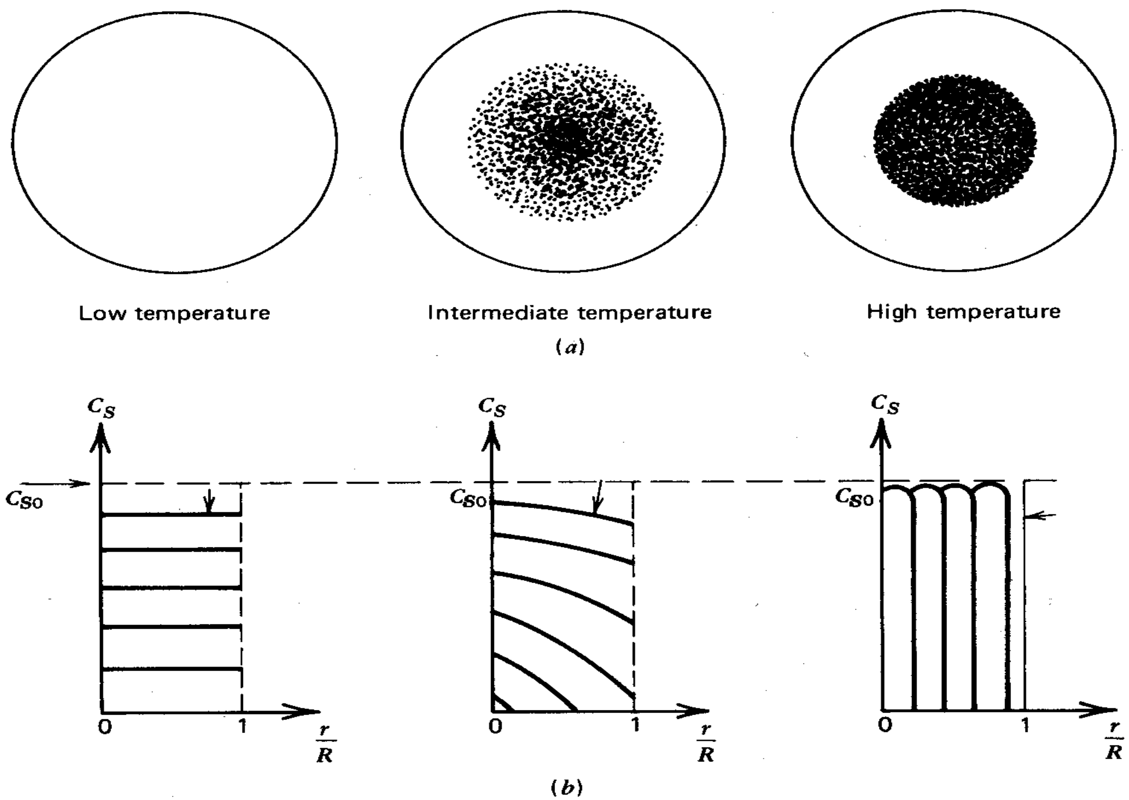

Figure 2
Appearance after partial burnoff (*a*) and coke concentration versus radius in beads for successive stages of burnoff (*b*), for three temperature levels. From Weisz and Goodwin (1963).

Burning of coke

$$t = \frac{R\rho_s}{3C_{1b}k_g}X + \frac{R^2\rho_s}{6C_{1b}D_{1e}}\left[1 - 3(1-X)^{2/3} + 2(1-X)\right] + \frac{R\rho_s}{kC_{1b}}\left[1 - (1-X)^{1/3}\right]$$

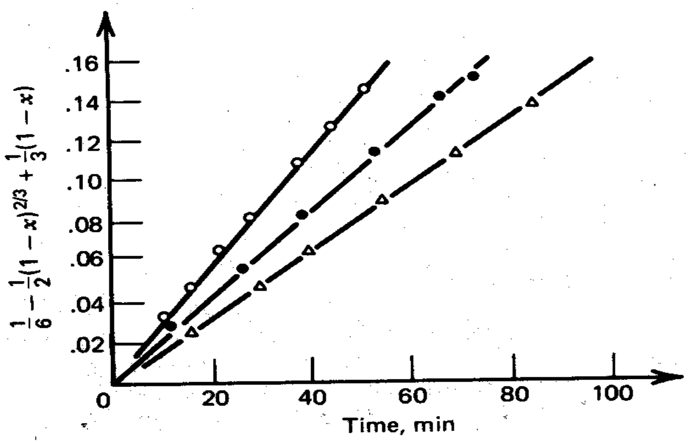

Figure 3
Burnoff function versus time for three different diameter beads. From Weisz and Goodwin (1963).

Time required for burning of coke

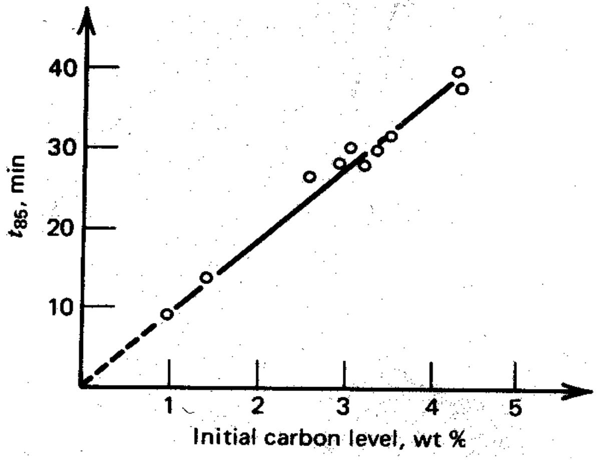

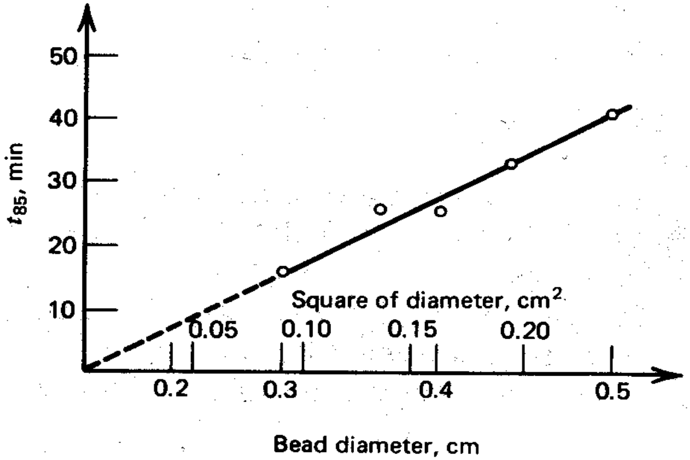

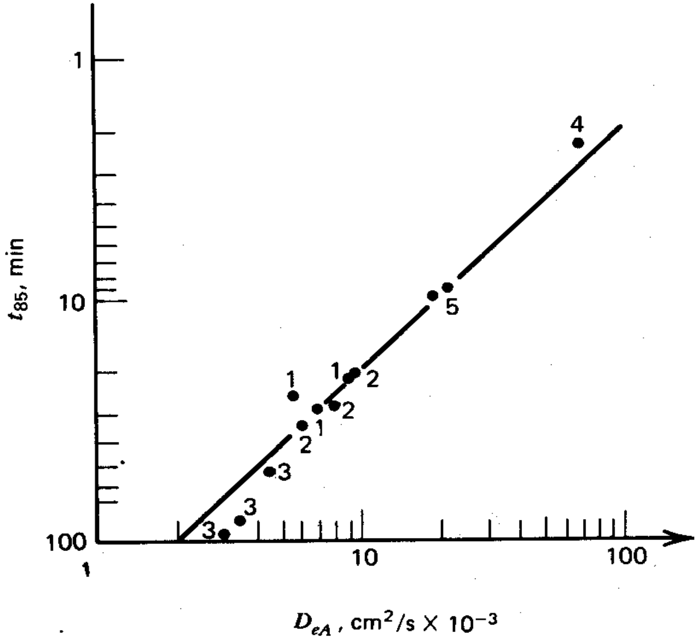

Gas-solid reaction: General Model – f = 1

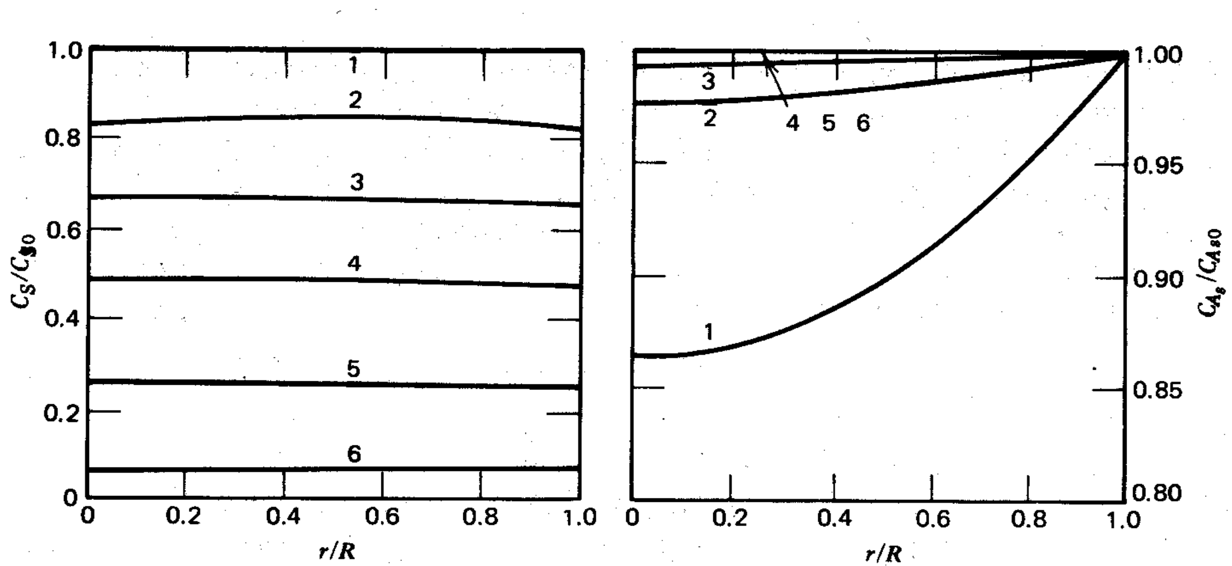

Curve	θ	x
1	0	0
2	0.189	0.165
3	0.429	0.341

Curve	θ	x
4	0.749	0.521
5	1.389	0.748
6	2.669	0.930

Figure 4.2-1
General model. Concentration profiles for $\phi'' = 1$. From Wen (1968).

Gas-solid reaction: General Model – f = 70

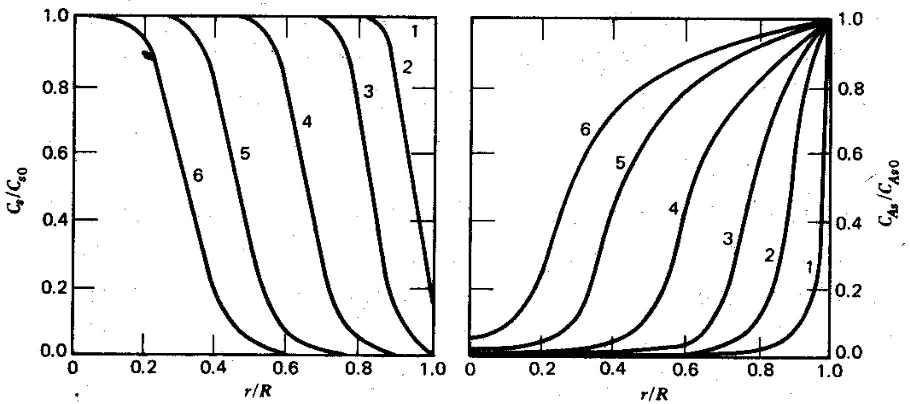

Curve	θ	x
1	0	0
2	1.84	0.151
3	4.88	0.417
4	10.16	0.708
5	16.40	0.892
6	20.56	0.957

Figure 4.2-2
General model. Concentration profiles for $\phi'' = 70$. From Wen (1968).

Gas-liquid reactions

- gas purification processes
  - CO_2 removal from synthesis gas by aqueous solution of hot potassium carbonate, ethanolamines
  - Removal of H_2S by ethanolamines or sodium hydroxide
- production processes
  - Air oxidation of aldehydes to acids
  - Oxidation of cyclohexane to adipic acid
  - chlorination of benzene
  - Nitric acid, sulphuric acid

Examples

Table 6.3.d-2 Characteristic parameters of some industrial gas-liquid reactions (from Barona [6]).

Reaction	T (°C)	C_{Ai} (kmol/m³)	C_{Bb} (kmol/m³)	Catalyst	Cat. conc. (kmol/m³)	D_A (m²/m·hr)	k_L (m³/m² hr)	k	γ
Chlorinations									
$B + Cl_2 \rightarrow CB + HCl$	80		10.45	$FeCl_3$		2.027×10^{-5}	1.303	4.143 m³/kmol hr	0.0227
id.	20	0.1245	11.22	$SnCl_4$	0.049	1.059×10^{-5}	0.716	43.09 m³/kmol hr	0.0999
$TCE + Cl_2 \rightarrow C_2H_2Cl_4 + HCl$	70		10.28			8.856×10^{-5}	0.576	4.619 m³/kmol hr	0.0357
$1PB + Cl_2 \rightarrow MC + HCl$	20	0.1750	7.183	$SnCl_4$	0.012	1.099×10^{-5}	0.734	850.6 m³/kmol hr	0.333
$EB + Cl_2 \rightarrow MC + HCl$	20	0.1060	8.179	$SnCl_4$	0.00708	1.234×10^{-5}	0.828	2087 m³/kmol hr	0.554
$T + Cl_2 \rightarrow MC + HCl$	20	0.1135	9.457	$SnCl_4$	0.00036	1.309×10^{-5}	0.828	3468 m³/kmol hr	0.791
$p\text{-}X + Cl_2 \rightarrow MC + HCl$	20	0.0685	8.066	$SnCl_4$	0.00066	1.234×10^{-5}	0.698	14430 m³/kmol hr	1.718
$o\text{-}X + Cl_2 \rightarrow MC + HCl$	20	0.1100	8.311	$SnCl_4$	0.00066	1.008×10^{-5}	0.796	16050 m³/kmol hr	1.464
Oxidations									
$THF + O_2 \rightarrow HP$	65		12.35	ADBN	0.06	2.131×10^{-5}	1.145	0.0138 hr⁻¹	0.00047
$EB + O_2 \rightarrow HP$	80			Cu^{II}-Stearate	1.62×10^{-5}	3.097×10^{-5}	1.498	0.000375 hr⁻¹	0.00073
id.	80		7.736	Cu^{II}-Stearate	0.056	3.097×10^{-5}	1.498	2.627 m³/kmol hr	0.0170
$o\text{-}X + O_2 \rightarrow o\text{-}TA$	160					5.389×10^{-5}	0.929	0.1025 m³/kmol hr	0.258

B: benzene; MCB: monochlorobenzene; TCE: 1,1,2-trichloroethane; 1PB: 1-propylbenzene; EB: ethylbenzene; T: toluene; *p*-X: *p*-Xylene; *o*-X: *o*-xylene; MC: monochloride of 1PB, EB, T, *p*-X, and *o*-X; THF: tetrahydrofurane; HP: hydroperoxide; *o*-TA: *o*-toluic acid; ADBN: azodiiso butyronitrile

Two-film model

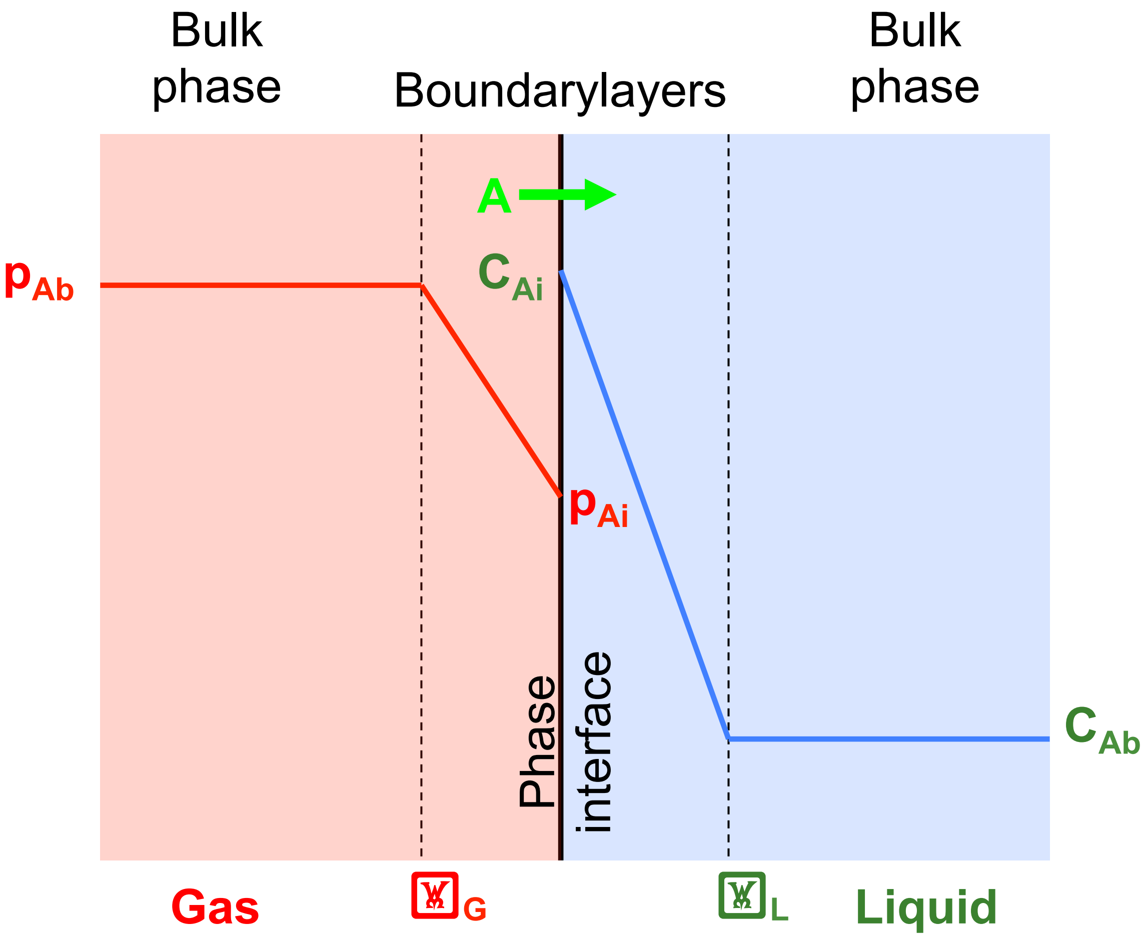

- masstransfer localised in surfacefilms
- C_{Ai} & p_{Ai} at equilibrium
- continuity of interfacial flux
- no reaction ⇒ const. slope

Slow reaction

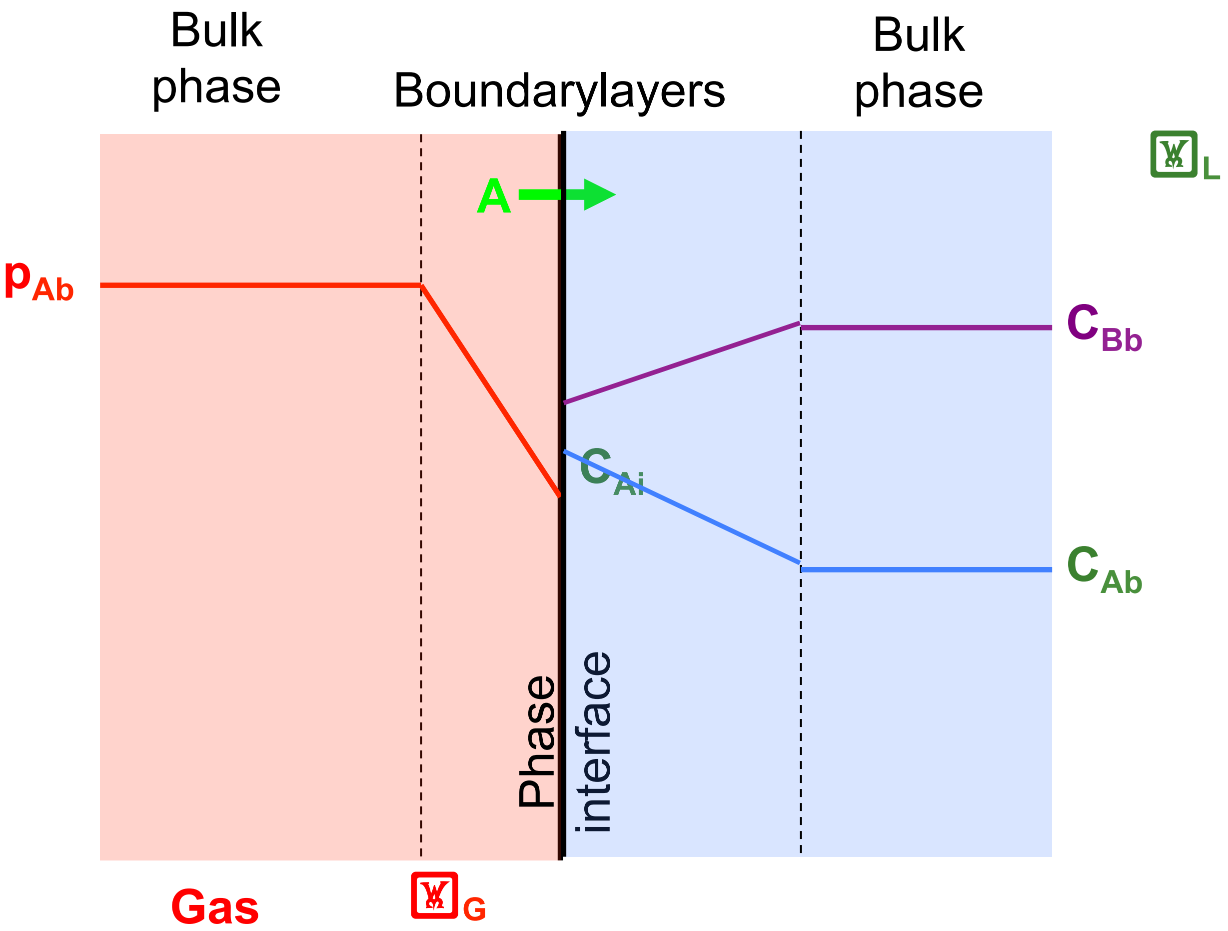

Moderate reaction

A(g) + B(aq) → C(aq)

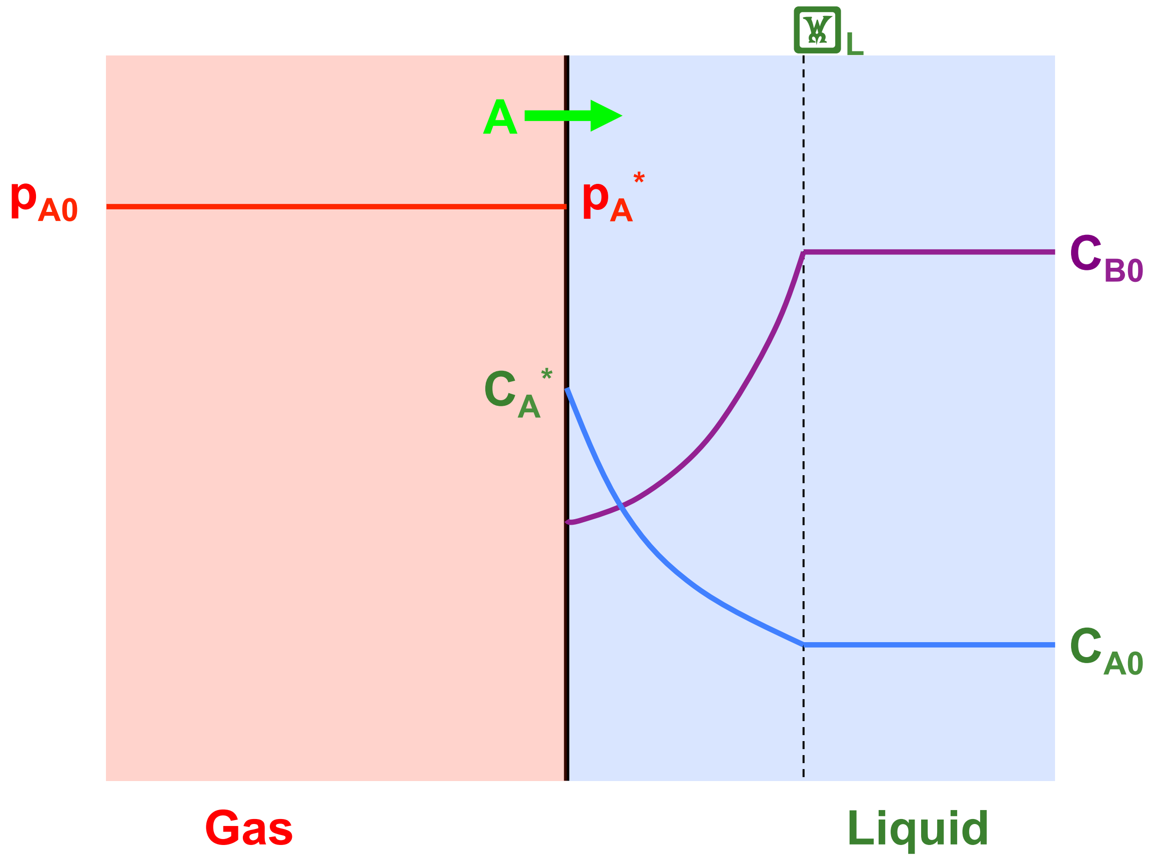

Fast reaction

A(g) + B(aq) [symbol] C(aq)

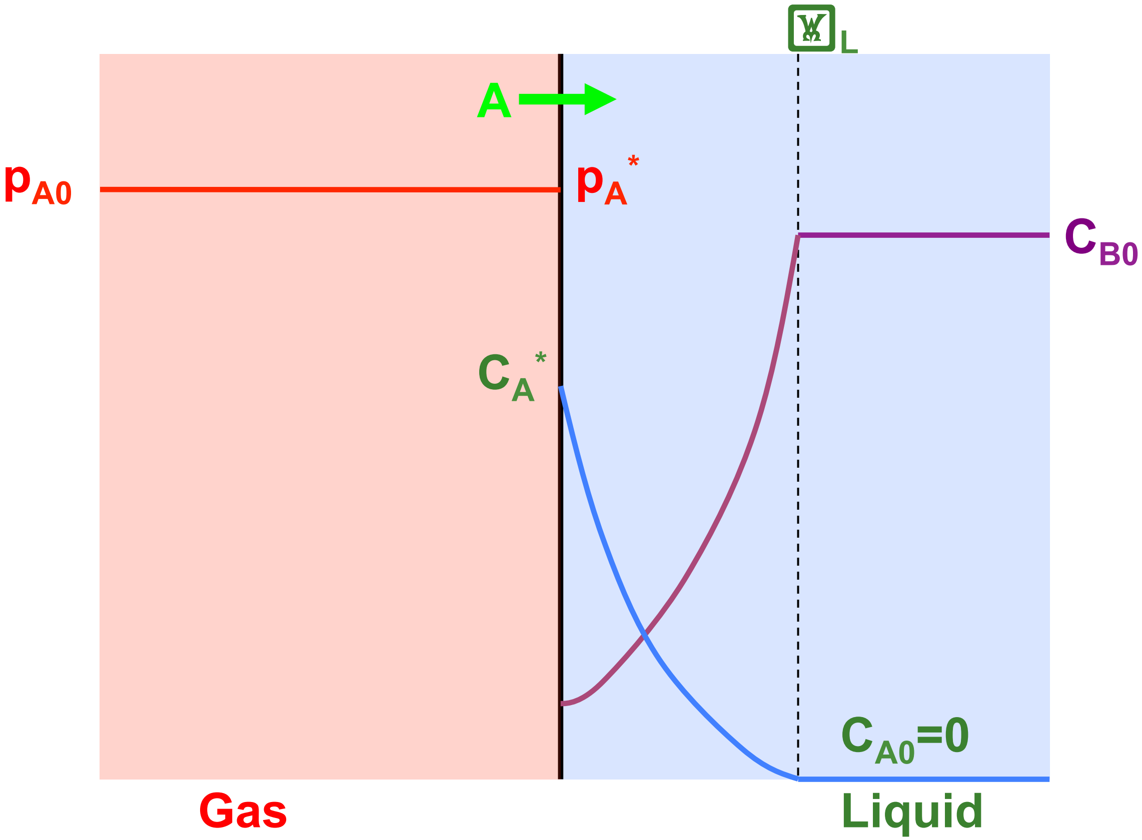

Fast reaction

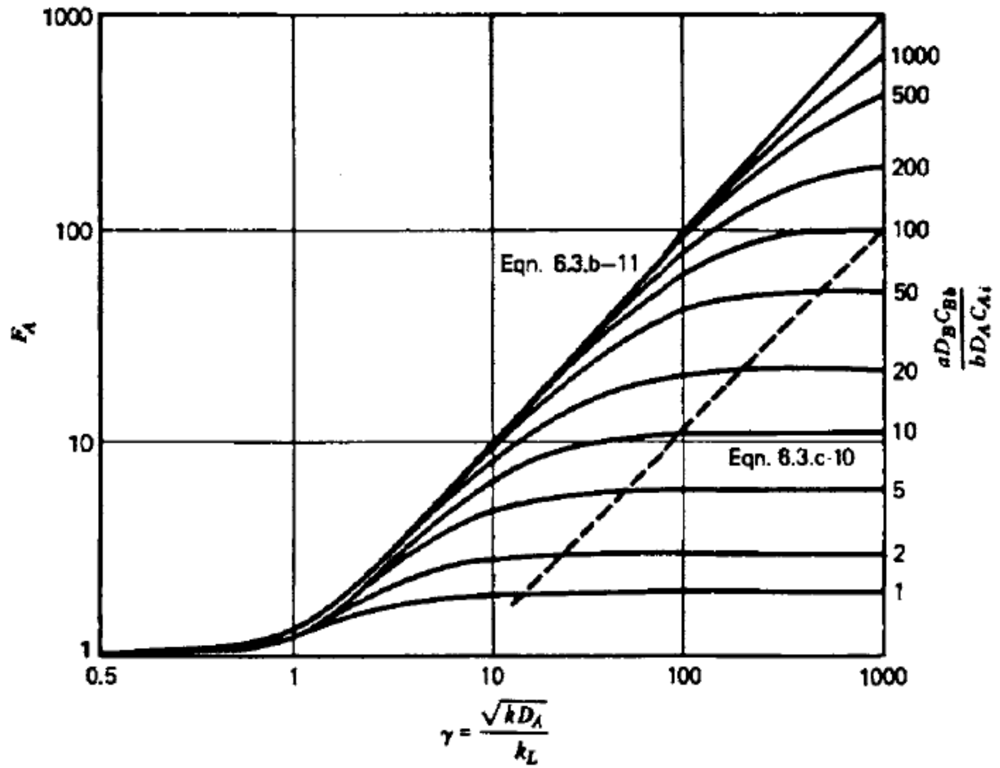

Figure 6.3.b-1 Enhancement factor diagram for $C_{Ab} = 0$.

Very Fast reaction

A(g) + B(aq) [symbol] C(aq)

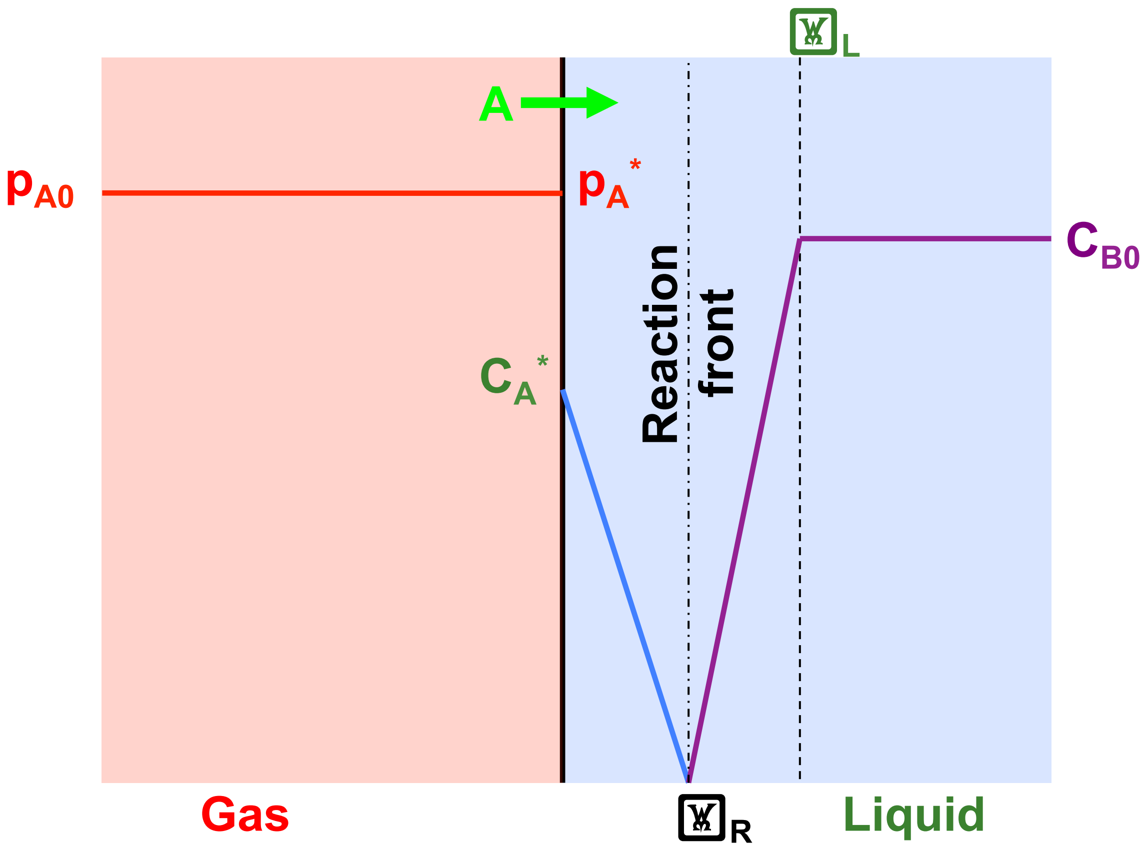

Instantaneous reaction

$A(g) + B(aq) \rightarrow C(aq)$